J|A|C|S COMMUNICATIONS

Published on Web 07/30/2010

Water Oxidation by λ-MnO_2: Catalysis by the Cubical Mn_4O_4 Subcluster Obtained by Delithiation of Spinel $LiMn_2O_4$

David M. Robinson, Yong Bok Go, Martha Greenblatt,* and G. Charles Dismukes*

Department of Chemistry and Chemical Biology, Rutgers, The State University of New Jersey, Piscataway, New Jersey 08854

Received June 24, 2010; E-mail: dismukes@rci.rutgers.edu; martha@rutchem.rutgers.edu

Abstract: Nanocrystalline spinel $LiMn_2O_4$ has been prepared and treatment of $LiMn_2O_4$ with dilute nitric acid solution resulted in the delithiation of the framework, while maintaining the spinel structure, λ-MnO_2. $LiMn_2O_4$ is not a catalyst for water oxidation. Upon removal of the lithium, the cubical Mn_4O_4 cores become active sites for oxidizing water to molecular oxygen, which was investigated with the photochemical [Ru^{2+}(2,2′-bpy)$_3$]/persulfate system at pH 5.8. The nanosize λ-MnO_2 obtained from the nanocrystalline $LiMn_2O_4$, which was synthesized by the citrate route, shows a significantly higher water oxidation catalytic activity (Turnover Frequency: 3×10^{-5} mol O_2/s/mol Mn) than that obtained via solid state reaction with micrometer and irregular particle sizes (Turnover Frequency: 5×10^{-6} mol O_2/s/mol Mn).

New catalysts made from inexpensive and abundant materials are needed to replace precious metals currently used in commercial water electrolyzers for the production of hydrogen and oxygen. RuO_2 and IrO_2 are the most widely used in commercial electrolyzers,[1] despite their limited availability and high cost. Many efforts have sought to understand and develop the potential of these materials.[2−4]

Another approach taken thus far for the oxygen evolving half-cell reaction (OER, eq 1) is to model catalysts upon the photosystem II water-oxidizing complex (PSII-WOC), found within photosynthetic organisms.

$$2H_2O(l) \rightarrow O_2(g) + 4H^+(sol) + 4e^- \quad (1)$$

The universally conserved catalytic core of this enzyme is comprised of a cubical $CaMn_3O_4$ cluster and a fourth Mn atom bridged via an oxygen atom.[5,6] The chemical principles that may govern catalysis by this inorganic core have been studied through development of homogeneous water oxidation catalysts that are structurally related, including cubical Mn_4O_4 core molecules[7,8] and less related Mn_2O_2 core molecules.[9,10]

In addition, metal oxides of various compositions and allotropes have been studied for water oxidation potential, including spinels which exhibit low catalytic activity in the bulk phase.[4,11] Recently spinel-type Co_3O_4 nanoparticles have demonstrated enhanced catalytic capabilities relative to the bulk phase.[12,13] Although manganese oxides (Mn_2O_3 and rutile MnO_2) have shown little success in water oxidation trials,[4,11,14] the concepts learned from the PSII-WOC and the Mn_4O_4 core complex encourage further studies of these materials.

Herein, we examine the possibility of activating the B site cations in AB_2O_4 spinels for catalysis by removal of the A site cations. Because the B cations are arrayed as B_4O_4 cubes resembling the PSII-WOC and the Mn_4O_4-cubanes, we are testing whether the cubical topology is the common feature for catalysis of water oxidation. We report the first observation, to our knowledge, that removal of the Li cation from $LiMn_2O_4$ converts this inactive spinel to a water oxidation catalyst.

$LiMn_2O_4$ is a highly studied material used as a cathode in rechargeable batteries with many nanoscale synthesis procedures. It has a spinel type structure with Mn^{III} and Mn^{IV} ions occupying the octahedral B sites and Li ions in the tetrahedral A sites as seen in Figure 1.

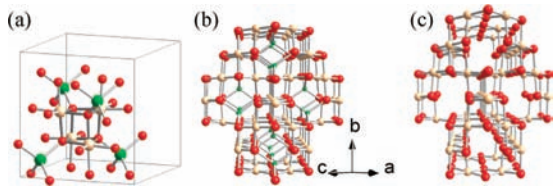

Figure 1. Perspective view of (a) a cubane core in the unit cell of spinel $LiMn_2O_4$, (b) an extended three-dimensional framework structure of $LiMn_2O_4$, and (c) λ-MnO_2 with void spaces after removal of Li ions. Li, Mn, and O atoms are shown as green, pink, and red, respectively.

The exchange properties of Li^+ from $LiMn_2O_4$ are well understood.[15−17] Li^+ can be fully removed from the spinel framework yielding an allotrope of MnO_2 denoted λ-MnO_2. This material retains the spinel framework but with empty A sites, resulting in a uniquely open structure. λ-MnO_2 is not found naturally and differs from the common allotrope β-MnO_2 (rutile structure, with all O atoms tricoordinate). The B cations in λ-MnO_2 and $LiMn_2O_4$ are organized as cubical Mn_4O_4 subunits that are linked to the other B site cations via oxo bridges (exclusively dicoordinate in λ-MnO_2). The cubical Mn_4O_4 units in λ-MnO_2 are topologically similar to the Mn_4O_4 core found in the molecular "cubane" catalysts used for water oxidation and indirectly the $CaMn_4O_4$ core of the PSII-WOC structure.

We used two synthetic procedures to generate nanoscale $LiMn_2O_4$, which are described in the Supporting Information. Briefly, the first procedure utilizes a high temperature (850 °C, **HT**) route with Li_2CO_3 and Mn_2O_3.[17] The second combines $Mn(OAc)_2$ with $LiNO_3$ at a lower temperature (350 °C, **LT**) in the presence of urea and citrate in acidic solution to aid in forming a higher surface area material during degassing of H_2O, NH_3, and CO_2.[18] Removal of the Li^+ is performed by dilute HNO_3 solution treatment[17] as described below and in the Supporting Information. The acid treatment (eq 2) dissolves the Li_2O and MnO products of the reaction and yields a solid that analyzes gravimetrically as λ-MnO_2 with 100% removal of Li^+.

$$2LiMn_2O_4(s) \xrightarrow{HNO_3(sol)} Li_2O(s) + 3\lambda\text{-}MnO_2(s) + MnO(s) \quad (2)$$

Powder X-ray diffraction verifies the formation of spinel $LiMn_2O_4$ and reveals that the spinel spacing is maintained in

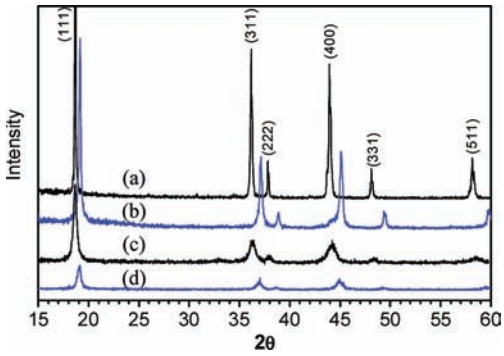

Figure 2. X-ray diffraction patterns of (a) $LiMn_2O_4$ (**HT**), (b) λ-MnO_2 (**HT**), (c) $LiMn_2O_4$ (**LT**), and (d) λ-MnO_2 (**LT**). Diffraction peaks of the λ-MnO_2 material show an equivalent upshift of 2θ.

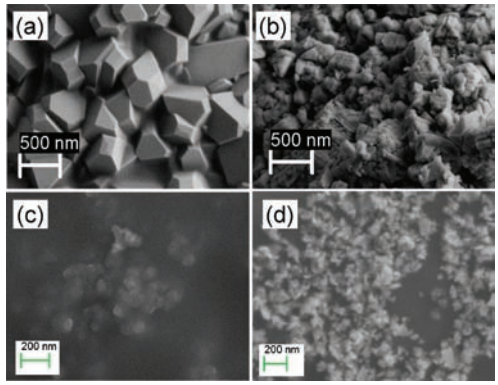

Figure 3. SEM images of (a) $LiMn_2O_4$ (**HT**), (b) λ-MnO_2 (**HT**), (c) $LiMn_2O_4$ (**LT**), and (d) λ-MnO_2 (**LT**).

λ-MnO_2 after delithiation as shown in Figure 2. All diffraction peaks of the λ-MnO_2 material show an equivalent upshift of 2θ equal to about 3% and broadening, while maintaining the spinel pattern as reported in the literature.[17] The retention of the spinel pattern and complete delithiation upon acid treatment confirm the λ phase MnO_2 material. Upon removal of the A site atoms, the cubical structure highlighted in Figure 1a is maintained while creating nanochannels with an approximate dimension of 4 Å × 3 Å (Figure 1c).

Scanning Electron Microscopy (SEM) of the product of the high temperature method reveals crystallite particle sizes ranging from 200 to 500 nm in diameter (Figure 3). The treatment of the high temperature material with HNO_3 produced a delithiated material with a fractured crystal structure and visible imperfections on the crystal faces. The low temperature synthesis produces a wide range of sizes and more irregular crystallites with the smallest feature at ~20 nm, as seen in the SEM and confirmed by the peak width in XRD. The crystallite size of the $LiMn_2O_4$ (**LT**) and λ-MnO_2 (**LT**) powders was calculated by Scherrer's formula with the full width at half-maximum data of the (111) plane observed at 18.68° 2θ, yielding an average crystallite size of ~22 and ~19 nm, respectively.

Scheme 1. Photon Driven Oxidation System Used for Solution Phase Water Oxidation Experiments: One Electron per Turnover Ru^{III}/Ru^{II}

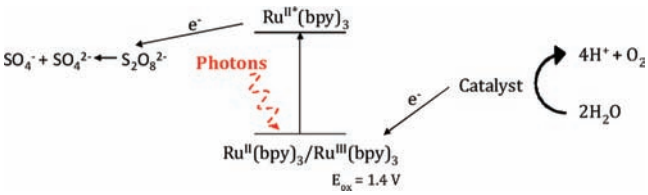

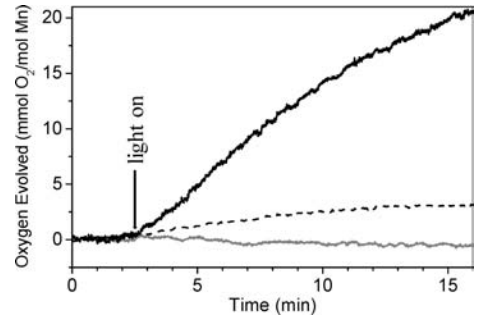

Figure 4. Oxygen evolution by Clark electrode measurements for λ-MnO_2 (**LT**; black), λ-MnO_2 (**HT**; dashed), and $LiMn_2O_4$(gray).

Catalytic water oxidation was monitored in solution through detection of dissolved O_2 by thermostatted Clark-type electrode and confirmed by gas chromatography as described in the Supporting Information. Oxidative equivalents were provided upon illumination through a standard photoexcitation system dissolved in water[12] as depicted in Scheme 1.

Oxygen concentrations were recorded for over 15 min upon illumination as shown in Figure 4, from which initial rates were determined. Separate experiments were performed with reaction solutions without each of the key components of the photocatalytic system (catalyst, $Ru(bpy)_3^{2+}$, light, persulfate) yielding no oxygen evolution. The requirement for a complete system for oxygen evolution indicates the reaction requires each of these components.

Figure 4 clearly shows that removal of Li from the $LiMn_2O_4$ structure creates a catalytically active λ-MnO_2 material from an otherwise inactive spinel. Neither the **HT** nor **LT** $LiMn_2O_4$ material exhibits activity in water oxidation. However, by decreasing particle size and morphology of the λ-MnO_2 material from 200−500 nm (**HT**) to ca. 20−100 nm (**LT**) (Figure 3) there is a 6-fold increase in the initial rate of O_2 evolution, suggesting that surface accessibility to the photocatalytic system limits the turnover rate. The one-dimensional channels produced within the λ-MnO_2 (4 Å × 3 Å, Figure 1) are not large enough for permeation of the $Ru(bpy_3)^{3+}$ oxidizing agent. Thus only the surface Mn species likely participate in the photoreaction, and removal of Li and particle size are the mechanistically important attributes for catalysis at the atomic level.

Table 1. Turnover Frequency (TOF) Numbers for Various Mn- and Co-Based Bulk Catalysts (mol O_2/s/mol). In Parenthesis are Surface Mn or Co (mol O_2/s/mol)

Catalyst Material	TOF (s^{-1})
λ-MnO_2 (**HT**)	5×10^{-6} (0.001)[a]
λ-MnO_2 (**LT**)	3×10^{-5} (?)[a]
SBA-15/Co_3O_4 (4%)[12]	NA (0.01)
Co_3O_4 nanocubes[13]	0.09 (0.12)[b]
$Mn_2O_2(terpy)_2(OH_2)_2$[9]	5×10^{-5} (NA)
$Mn_4O_4(MeOPh_2PO_2)$/Nafion[8]	2.4×10^{-4} (NA)

[a] The intrinsic TOF for λ-MnO_2 is higher, because in our method the rate is limited by the photogeneration of Ru^{III}. [b] All TOF values are at neutral pH except for Co_3O_4 nanocubes (ref 13), which is at pH 14 (5 M KOH) and an overpotential of 388 mV.

Initial oxygen evolution rates for the λ-MnO_2 (**LT** and **HT**) are given in Table 1. The values calculated for oxygen evolution rates correspond to low end estimates for turnover based on every Mn atom catalytically active. For the **HT** phase we estimate a TOF of 1×10^{-3} s^{-1} per surface Mn atom, based upon the surface/volume ratio of the crystallites (Supporting Information). The value for TOF per surface Mn for λ-MnO_2 (**HT**) is 10 times lower than that for the much smaller SBA-15/Co_3O_4 spinel (7.6 nm ×50 nm) (Table

1), which represents a dilute solid-state solution, not a concentrated solid like λ-MnO_2.[12] Comparisons to other well characterized catalytic water splitting systems (Table 1) reveal that λ-MnO_2 is an important step toward a robust Mn-based water-oxidizing catalyst that uses nontoxic, earth-abundant materials. We conclude that the cubical B_4O_4 unit in spinels can be activated by removal of structural Li^+, which introduces flexibility as the important degree of freedom for catalysis. This design principle is analogous to that believed to operate in the PSII-WOC and molecular cubanes.[8]

Acknowledgment. Supported by Rutgers University and AFOSR-FA9550-05-1-0365. M.G. and Y.B.G. acknowledge partial support by NSF-DMR-0541911 and 0966829. We thank Dr. Steve Miller for SEM images.

Supporting Information Available: Synthesis procedures for $LiMn_2O_4$ and λ-MnO_2. Experimental details for oxygen evolution procedure. This material is available free of charge via the Internet at http://pubs.acs.org.

References

(1) Marshall, A. T.; Haverkamp, R. G. *Electrochim. Acta* **2010**, *55*, 1978–1984.
(2) Morris, N. D.; Suzuki, M.; Mallouk, T. E. *J. Phys. Chem. A* **2004**, *108*, 9115–9119.
(3) Yagi, M.; Tomita, E.; Sakita, S.; Kuwabara, T.; Nagai, K. *J. Phys. Chem. B* **2005**, *109*, 21489–21491.
(4) Harriman, A.; Pickering, I. J.; Thomas, J. M.; Christensen, P. A. *J. Chem. Soc., Faraday Trans. 1* **1988**, *84*, 2795–2806.
(5) Ferreira, K. N.; Iverson, T. M.; Maghlaoui, K.; Barber, J.; Iwata, S. *Science* **2004**, *303*, 1831–1838.
(6) Barber, J.; Murray, J. W. *Coord. Chem. Rev.* **2008**, *252*, 233–243.
(7) Brimblecombe, R.; Kolling, D. R. J.; Bond, A. M.; Dismukes, G. C.; Swiegers, G. F.; Spiccia, L. *Inorg. Chem.* **2009**, *48*, 7269–7279.
(8) Dismukes, G. C.; Brimblecombe, R.; Felton, G. A. N.; Pryadun, R. S.; Sheats, J. E.; Spiccia, L.; Swiegers, G. F. *Acc. Chem. Res.* **2009**, *42*, 1935–1943.
(9) Yagi, M.; Narita, K. *J. Am. Chem. Soc.* **2004**, *126*, 8084–8085.
(10) Limburg, J.; Vrettos, J. S.; Chen, H. Y.; de Paula, J. C.; Crabtree, R. H.; Brudvig, G. W. *J. Am. Chem. Soc.* **2001**, *123*, 423–430.
(11) Parmon, V. N.; Elizarova, G. L.; Kim, T. V. *React. Kinet. Catal. Lett.* **1982**, *21*, 195–197.
(12) Jiao, F.; Frei, H. *Angew. Chem., Int. Ed.* **2009**, *48*, 1841–1844.
(13) Esswein, A. J.; McMurdo, M. J.; Ross, P. N.; Bell, A. T.; Tilley, T. D. *J. Phys. Chem. C* **2009**, *113*, 15068–15072.
(14) Luneva, N. P.; Shafirovich, V. Y.; Shilov, A. E. *J. Mol. Catal.* **1989**, *52*, 49–62.
(15) Thackeray, M. M.; David, W. I. F.; Bruce, P. G.; Goodenough, J. B. *Mater. Res. Bull.* **1983**, *18*, 461–472.
(16) Koyanaka, H.; Matsubaya, O.; Koyanaka, Y.; Hatta, N. *J. Electroanal. Chem.* **2003**, *559*, 77–81.
(17) Hunter, J. C. *J. Solid State Chem.* **1981**, *39*, 142–147.
(18) Vivekanandhan, S.; Venkateswarlu, M.; Satyanarayana, N. *J. Alloys Compd.* **2007**, *441*, 284–290.

JA1055615